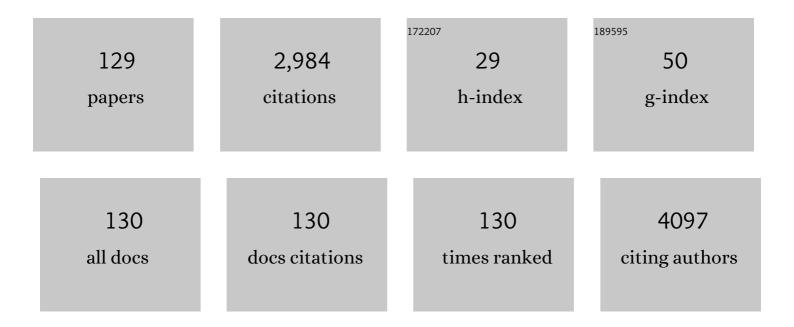
List of Publications by Year in descending order

Source: https://exaly.com/author-pdf/5717772/publications.pdf Version: 2024-02-01



#	Article	IF	CITATIONS
1	Rational Functionalization of UiO-66 with Pd Nanoparticles: Synthesis and In Situ Fourier-Transform Infrared Monitoring. Inorganic Chemistry, 2022, 61, 3875-3885.	1.9	8
2	How Much Structural Information Could Be Extracted from XANES Spectra for Palladium Hydride and Carbide Nanoparticles. Journal of Physical Chemistry C, 2022, 126, 4921-4928.	1.5	7
3	Cobalt nanoparticles embedded in porous N-doped carbon support as a superior catalyst for the p-nitrophenol reduction. Applied Surface Science, 2022, 592, 153292.	3.1	17
4	Improvement of the EC Performance in LCP-MOF Electrode Materials by Succinic Anhydrate Addition to the Electrolyte. Sustainability, 2022, 14, 323.	1.6	0
5	Laboratory X-ray Microscopy Study of Microcrack Evolution in a Novel Sodium Iron Titanate-Based Cathode Material for Li-Ion Batteries. Crystals, 2022, 12, 3.	1.0	3
6	Chemical Information in the L ₃ X-ray Absorption Spectra of Molybdenum Compounds by High-Energy-Resolution Detection and Density Functional Theory. Inorganic Chemistry, 2022, 61, 869-881.	1.9	3
7	Facile synthesis of ZnNC derived from a ZIF-8 metal-organic framework by the microwave-assisted solvothermal technique as an anode material for lithium-ion batteries. New Journal of Chemistry, 2022, 46, 9138-9145.	1.4	6
8	Iron (II) fluoride cathode material derived from MIL-88A. Journal of Alloys and Compounds, 2022, 916, 165438.	2.8	10
9	Hydrogenation of ethylene over palladium: evolution of the catalyst structure by operando synchrotron-based techniques. Faraday Discussions, 2021, 229, 197-207.	1.6	9
10	Structural Changes in Fiveâ€Coordinate Bromidoâ€bis(oâ€iminobenzoâ€semiquinonato)iron(III) Complex: Spinâ€Crossover or Ligandâ€Metal Antiferromagnetic Interactions?. European Journal of Inorganic Chemistry, 2021, 2021, 756-762.	1.0	1
11	Kramers-Kronig analysis of the optical linearity and nonlinearity of nanostructured Ga-doped ZnO thin films. Optics and Laser Technology, 2021, 135, 106691.	2.2	20
12	Application of Ligand Field Theory for Simulation of the Pre-Edge Structure of X-Ray Absorption Spectra of Amorphous Systems. Journal of Surface Investigation, 2021, 15, 1-6.	0.1	0
13	Laboratory Operando XAS Study of Sodium Iron Titanite Cathode in the Li-Ion Half-Cell. Nanomaterials, 2021, 11, 156.	1.9	7
14	Activation of LiCoPO4 in Air. Journal of Electronic Materials, 2021, 50, 3105-3110.	1.0	4
15	Quantitative Analysis of the UV–Vis Spectra for Gold Nanoparticles Powered by Supervised Machine Learning. Journal of Physical Chemistry C, 2021, 125, 8656-8666.	1.5	19
16	Valence tautomeric transition of bis(o-dioxolene) cobalt complex in solid state and solution. Journal of Physics Condensed Matter, 2021, 33, 215405.	0.7	9
17	Quantitative Analysis of X-Ray Spectral Data for a Mixture of Compounds Using Machine-Learning Algorithms. Journal of Surface Investigation, 2021, 15, 495-501.	0.1	1
18	Deciphering the Phillips Catalyst by Orbital Analysis and Supervised Machine Learning from Cr Pre-edge XANES of Molecular Libraries. Journal of the American Chemical Society, 2021, 143, 7326-7341.	6.6	26

#	Article	IF	CITATIONS
19	XAS Diagnostic of the Photoactive State in Co(II) Azobenzene Complex in Organic Solvents. ChemistrySelect, 2021, 6, 7087-7092.	0.7	0
20	Enhanced Reducibility of the Ceria–Tin Oxide Solid Solution Modifies the CO Oxidation Mechanism at the Platinum–Oxide Interface. ACS Catalysis, 2021, 11, 9435-9449.	5.5	19
21	Revisiting the Extended X-ray Absorption Fine Structure Fitting Procedure through a Machine Learning-Based Approach. Journal of Physical Chemistry A, 2021, 125, 7080-7091.	1.1	15
22	Enhancement of the electrochemical performance of LiCoPO4 by Fe doping. Ceramics International, 2021, 47, 31826-31833.	2.3	10
23	Machine learning powered by principal component descriptors as the key for sorted structural fit of XANES. Physical Chemistry Chemical Physics, 2021, 23, 17873-17887.	1.3	7
24	Estimating a Set of Pure XANES Spectra from Multicomponent Chemical Mixtures Using a Transformation Matrix-Based Approach. Springer Proceedings in Physics, 2021, , 65-84.	0.1	7
25	Search for Analytical Relations between X-Ray Absorption Spectra Descriptors and the Local Atomic Structure Using Machine Learning. Journal of Surface Investigation, 2021, 15, 934-938.	0.1	5
26	Temperature and Time-resolved XANES Studies of Novel Valence Tautomeric Cobalt Complex. Chemistry Letters, 2021, 50, 1933-1937.	0.7	7
27	Revisited Ti ₂ Nb ₂ O ₉ as an Anode Material for Advanced Li-Ion Batteries. ACS Applied Materials & Interfaces, 2021, 13, 56366-56374.	4.0	8
28	Excited-state structure of copper phenanthroline-based photosensitizers. Physical Chemistry Chemical Physics, 2021, 23, 26729-26736.	1.3	6
29	Understanding X-ray absorption spectra by means of descriptors and machine learning algorithms. Npj Computational Materials, 2021, 7, .	3.5	48
30	Complex diagnostics of ordinary chondrites Markovka, Polujamki, Sayh al Uhaymir 001, Dhofar 020, and Jiddat al Harasis 055 by Xâ€ray techniques and Mössbauer spectroscopy. Meteoritics and Planetary Science, 2021, 56, 2191-2210.	0.7	0
31	Speciation of Ru Molecular Complexes in a Homogeneous Catalytic System: Fingerprint XANES Analysis Guided by Machine Learning. Journal of Physical Chemistry C, 2021, 125, 27844-27852.	1.5	9
32	Laboratory operando Fe and Mn K-edges XANES and Mössbauer studies of the LiFe0.5Mn0.5PO4 cathode material. Radiation Physics and Chemistry, 2020, 175, 108065.	1.4	8
33	X-ray and optical characterization of the intermediate products in the Au3+ reduction process by oleylamine. Radiation Physics and Chemistry, 2020, 175, 108067.	1.4	4
34	MLFT approach with p-d hybridization for ab initio simulations of the pre-edge XANES. Radiation Physics and Chemistry, 2020, 175, 108105.	1.4	5
35	Time-dependent carbide phase formation in palladium nanoparticles. Radiation Physics and Chemistry, 2020, 175, 108079.	1.4	17
36	Iron oxidation state of impact glasses from the Zhamanshin crater studied by X-ray absorption spectroscopy. Radiation Physics and Chemistry, 2020, 175, 108097.	1.4	7

#	Article	IF	CITATIONS
37	Machine learning approaches to XANES spectra for quantitative 3D structural determination: The case of CO2 adsorption on CPO-27-Ni MOF. Radiation Physics and Chemistry, 2020, 175, 108430.	1.4	21
38	First-principle calculation for inherent stabilities of LixCoPO4, NaxCoPO4 and the mixture LixNayCoPO4. Journal of Physics and Chemistry of Solids, 2020, 136, 109192.	1.9	5
39	New orthorhombic sodium iron(+2) titanate. Ceramics International, 2020, 46, 4416-4422.	2.3	6
40	Zn–F co-doped TiO2 nanomaterials: Synthesis, structure and photocatalytic activity. Journal of Alloys and Compounds, 2020, 822, 153662.	2.8	35
41	Spin-crossover in the iron(II) complex based on dihydro-bis(pyrazolyl)borate and 1,10-phenanthroline-5,6-dione. Chemical Physics Letters, 2020, 739, 136970.	1.2	4
42	PyFitit: The software for quantitative analysis of XANES spectra using machine-learning algorithms. Computer Physics Communications, 2020, 250, 107064.	3.0	64
43	Theoretical Simulation of the Binding Energies and Stretching Frequencies of CO Molecules on PtSn Bimetallic Nanoparticles. Journal of Surface Investigation, 2020, 14, 440-446.	0.1	0
44	Synthesis and Description of Small Gold and Palladium Nanoparticles on CeO2 Substrate: FT- IR Spectroscopy Data. Journal of Surface Investigation, 2020, 14, 447-458.	0.1	2
45	Pd nanoparticle growth monitored by DRIFT spectroscopy of adsorbed CO. Analyst, The, 2020, 145, 7534-7540.	1.7	17
46	A novel α-Fe2O3@MoS2QDs heterostructure for enhanced visible-light photocatalytic performance using ultrasonication approach. Ceramics International, 2020, 46, 19600-19608.	2.3	21
47	XPS and XAS investigations of multilayer nanostructures based on the amorphous CoFeB alloy. Journal of Electron Spectroscopy and Related Phenomena, 2020, 243, 146979.	0.8	2
48	Elucidating the Oxygen Activation Mechanism on Ceria-Supported Copper-Oxo Species Using Time-Resolved X-ray Absorption Spectroscopy. ACS Catalysis, 2020, 10, 4692-4701.	5.5	21
49	Understanding the Origin of Higher Capacity for Ni-Based Disordered Rock-Salt Cathodes. Chemistry of Materials, 2020, 32, 3447-3461.	3.2	16
50	In Situ Time-Resolved Decomposition of \hat{l}^2 -Hydride Phase in Palladium Nanoparticles Coated with Metal-Organic Framework. Metals, 2020, 10, 810.	1.0	1
51	Absorption of Hydrocarbons on Palladium Catalysts: From Simple Models Towards Machine Learning Analysis of X-ray Absorption Spectroscopy Data. Topics in Catalysis, 2020, 63, 58-65.	1.3	14
52	Taking a snapshot of the triplet excited state of an OLED organometallic luminophore using X-rays. Nature Communications, 2020, 11, 2131.	5.8	24
53	Đ¡Đ,Đ½Ñ,ез Đ½Đ°Đ½Đ¾Ñ‡Đ°ÑŇ,Đ,ц ĐįаллаĐĐ,Ñ•Đ½Đ° ĐįĐ¾Đ²ĐµÑ€ÑĐ½Đ¾ÑŇ,Đ, Đ¾ĐºÑ	Ð,ÐÆÐ8ц [еÑt€Ð,Ñ (IV) (

⁵⁴ In situ X-ray absorption spectroscopy data during formation of active Pt- and Pd-sites in functionalized UiO-67 metal-organic frameworks. Data in Brief, 2019, 25, 104280.

0.5 3

#	Article	IF	CITATIONS
55	Kinetics of the Atomic Structure of Palladium Nanoparticles during the Desorption of Hydrogen According to X-Ray Diffraction. JETP Letters, 2019, 109, 594-599.	0.4	1
56	Suppressing Dissolution of Vanadium from Cation-Disordered Li _{2–<i>x</i>} VO ₂ F via a Concentrated Electrolyte Approach. Chemistry of Materials, 2019, 31, 7941-7950.	3.2	27
57	Rational Design of Grapheneâ€Supported Single Atom Catalysts for Hydrogen Evolution Reaction. Advanced Energy Materials, 2019, 9, 1803689.	10.2	279
58	Operando XAS and UV–Vis Characterization of the Photodynamic Spiropyran–Zinc Complexes. Journal of Physical Chemistry B, 2019, 123, 1324-1331.	1.2	12
59	Operando X-ray absorption spectra and mass spectrometry data during hydrogenation of ethylene over palladium nanoparticles. Data in Brief, 2019, 24, 103954.	0.5	8
60	Ultra-Small Pd Nanoparticles on Ceria as an Advanced Catalyst for CO Oxidation. Catalysts, 2019, 9, 385.	1.6	19
61	The effect of cobalt content in Zn/Co-ZIF-8 on iodine capping properties. Inorganica Chimica Acta, 2019, 492, 18-22.	1.2	25
62	Evolution of Pt and Pd species in functionalized UiO-67 metal-organic frameworks. Catalysis Today, 2019, 336, 33-39.	2.2	19
63	The role of palladium carbides in the catalytic hydrogenation of ethylene over supported palladium nanoparticles. Catalysis Today, 2019, 336, 40-44.	2.2	29
64	Synthesis of Palladium Nanoparticles on the Surface of Cerium(IV) Oxide under the Action of Ultraviolet Radiation and Their Characterization. Nanotechnologies in Russia, 2019, 14, 435-443.	0.7	0
65	Absorption spectra at the iodine 3d ionisation threshold following the CH _x I ⁺ (<i>x</i> = 0–3) cation sequence. Physical Chemistry Chemical Physics, 2019, 21, 25415-25424.	1.3	5
66	Comprehensive Investigation of Some Ordinary Chondrites Based on X-Ray Methods and MA¶ssbauer Spectroscopy. Journal of Surface Investigation, 2019, 13, 995-1004.	0.1	0
67	Quantitative structural determination of active sites from in situ and operando XANES spectra: From standard ab initio simulations to chemometric and machine learning approaches. Catalysis Today, 2019, 336, 3-21.	2.2	70
68	Partial and Complete Substitution of the 1,4-Benzenedicarboxylate Linker in UiO-66 with 1,4-Naphthalenedicarboxylate: Synthesis, Characterization, and H ₂ -Adsorption Properties. Inorganic Chemistry, 2019, 58, 1607-1620.	1.9	42
69	Palladium Carbide and Hydride Formation in the Bulk and at the Surface of Palladium Nanoparticles. Journal of Physical Chemistry C, 2018, 122, 12029-12037.	1.5	61
70	Photoabsorption of the molecular IH cation at the iodine <mml:math xmlns:mml="http://www.w3.org/1998/Math/MathML"><mml:mrow><mml:mn>3</mml:mn><mml:mi>dedge. Physical Review A, 2018, 97, .</mml:mi></mml:mrow></mml:math 	וו> נו∤וס וותו:r	mrow2>
71	Time-resolved operando studies of carbon supported Pd nanoparticles under hydrogenation reactions by X-ray diffraction and absorption. Faraday Discussions, 2018, 208, 187-205.	1.6	47
72	<i>Operando</i> study of palladium nanoparticles inside UiO-67 MOF for catalytic hydrogenation of hydrocarbons. Faraday Discussions, 2018, 208, 287-306.	1.6	46

5

#	Article	IF	CITATIONS
73	Insight from X-ray Absorption Spectroscopy to Octahedral/Tetrahedral Site Distribution in Sm-Doped Iron Oxide Magnetic Nanoparticles. Journal of Physical Chemistry C, 2018, 122, 8543-8552.	1.5	17
74	Investigation of the nanoscale two-component ZnS-ZnO heterostructures by means of HR-TEM and X-ray based analysis. Journal of Solid State Chemistry, 2018, 262, 264-272.	1.4	4
75	Experimental and theoretical study of hydrogen desorption process from Mn(BH4)2. Journal of Alloys and Compounds, 2018, 735, 277-284.	2.8	6
76	Structural Deformations During Cycling of the Conversion Cathode Nanocomposite Based on FeF3. Journal of Structural Chemistry, 2018, 59, 1719-1725.	0.3	0
77	Magnetic field-induced ferroelectricity in S = 1/2 kagome staircase compound PbCu3TeO7. Npj Quantum Materials, 2018, 3, .	¹ 1.8	25
78	A room-temperature growth of gold nanoparticles on MOF-199 and its transformation into the [Cu2(OH)(BTC)(H2O)] phase. Polyhedron, 2018, 154, 357-363.	1.0	13
79	Fluorescence-detected XAS with sub-second time resolution reveals new details about the redox activity of Pt/CeO ₂ catalyst. Journal of Synchrotron Radiation, 2018, 25, 989-997.	1.0	14
80	Structure and Properties of Ferroelectric Materials after Mechanoactivation. Bulletin of the Russian Academy of Sciences: Physics, 2018, 82, 909-912.	0.1	1
81	Zn/Co ZIF family: MW synthesis, characterization and stability upon halogen sorption. Polyhedron, 2018, 154, 457-464.	1.0	44
82	The insights from X-ray absorption spectroscopy into the local atomic structure and chemical bonding of Metal–organic frameworks. Polyhedron, 2018, 155, 232-253.	1.0	34
83	Design of Nickel-Based Cation-Disordered Rock-Salt Oxides: The Effect of Transition Metal (M = V, Ti,) Tj ETQq1 1 (Materials & Interfaces, 2018, 10, 21957-21964.).784314 4.0	rgBT /Overlo 37
84	In situ formation of hydrides and carbides in palladium catalyst: When XANES is better than EXAFS and XRD. Catalysis Today, 2017, 283, 119-126.	2.2	103
85	Tuning Pt and Cu sites population inside functionalized UiO-67 MOF by controlling activation conditions. Faraday Discussions, 2017, 201, 265-286.	1.6	31
86	Core–Shell Structure of Palladium Hydride Nanoparticles Revealed by Combined X-ray Absorption Spectroscopy and X-ray Diffraction. Journal of Physical Chemistry C, 2017, 121, 18202-18213.	1.5	67
87	Spectroscopic Methods in Catalysis and Their Application in Well-Defined Nanocatalysts. Studies in Surface Science and Catalysis, 2017, , 221-284.	1.5	3
88	Effect of Molecular Guest Binding on the d–d Transitions of Ni ²⁺ of CPO-27-Ni: A Combined UV–Vis, Resonant-Valence-to-Core X-ray Emission Spectroscopy, and Theoretical Study. Inorganic Chemistry, 2017, 56, 14408-14425.	1.9	22
89	Modulator Effect in UiO-66-NDC (1,4-Naphthalenedicarboxylic Acid) Synthesis and Comparison with UiO-67-NDC Isoreticular Metal–Organic Frameworks. Crystal Growth and Design, 2017, 17, 5422-5431.	1.4	55
90	Microwave-assisted synthesis of magnetic iron oxide nanoparticles in oleylamine–oleic acid solutions. Mendeleev Communications, 2017, 27, 487-489.	0.6	30

#	Article	IF	CITATIONS
91	Specific features of the atomic structure of metallic layers of multilayered (CoFeZr/SiO2)32 and (CoFeZr/a-Si)40 nanostructures with different interlayers. Physics of the Solid State, 2017, 59, 385-391.	0.2	1
92	Probing Structure and Reactivity of Metal Centers in Metal–Organic Frameworks by XAS Techniques. , 2017, , 397-430.		4
93	In situ analysis of the formation steps of gold nanoparticles by oleylamine reduction. Journal of Structural Chemistry, 2017, 58, 1403-1410.	0.3	1
94	Linear magnetoelectric effect in göthite, α-FeOOH. Scientific Reports, 2017, 7, 16410.	1.6	7
95	Finite difference method accelerated with sparse solvers for structural analysis of the metal-organic complexes. Journal of Physics: Conference Series, 2016, 712, 012004.	0.3	24
96	Valence determination of rare earth elements in lanthanide silicates by <i>L</i> ₃ -XANES spectroscopy. Journal of Physics: Conference Series, 2016, 712, 012096.	0.3	10
97	A XAFS study of the local environment and reactivity of Pt- sites in functionalized UiO-67 MOFs. Journal of Physics: Conference Series, 2016, 712, 012125.	0.3	10
98	Metal-organic frameworks: structure, properties, methods of synthesis and characterization. Russian Chemical Reviews, 2016, 85, 280-307.	2.5	300
99	Mechanistic Evaluation of a Nickel Proton Reduction Catalyst Using Time-Resolved X-ray Absorption Spectroscopy. Journal of Physical Chemistry C, 2016, 120, 20049-20057.	1.5	21
100	Tracking the Structural and Electronic Configurations of a Cobalt Proton Reduction Catalyst in Water. Journal of the American Chemical Society, 2016, 138, 10586-10596.	6.6	77
101	Structural and Spectroscopic Characterization of Reaction Intermediates Involved in a Dinuclear Co–Hbpp Water Oxidation Catalyst. Journal of the American Chemical Society, 2016, 138, 15291-15294.	6.6	49
102	X-ray Absorption Spectroscopy and Coherent X-ray Diffraction Imaging for Time-Resolved Investigation of the Biological Complexes: Computer Modelling towards the XFEL Experiment. Journal of Physics: Conference Series, 2016, 712, 012024.	0.3	0
103	Investigation of oxygen vacancies in CeO ₂ /Pt system with synchrotron light techniques. Journal of Physics: Conference Series, 2016, 712, 012064.	0.3	3
104	Hydride phase formation in carbon supported palladium hydride nanoparticles by <i>in situ</i> EXAFS and XRD. Journal of Physics: Conference Series, 2016, 712, 012032.	0.3	30
105	Development of a water based process for stable conversion cathodes on the basis of FeF3. Journal of Power Sources, 2016, 313, 213-222.	4.0	39
106	Microsecond Xâ€ray Absorption Spectroscopy Identification of Co ^I Intermediates in Cobaloximeâ€Catalyzed Hydrogen Evolution. Chemistry - A European Journal, 2015, 21, 15158-15162.	1.7	35
107	Group Ill–V and Il–VI Quantum Dots and Nanoparticles. Springer Series in Optical Sciences, 2015, , 247-268.	0.5	1
108	Li ⁺ intercalation in isostructural Li ₂ VO ₃ and Li ₂ VO ₂ F with O ^{2â^'} and mixed O ^{2â^'} /F ^{â^'} anions. Physical Chemistry Chemical Physics, 2015, 17, 17288-17295.	1.3	67

#	Article	IF	CITATIONS
109	Improved Voltage and Cycling for Li ⁺ Intercalation in Highâ€Capacity Disordered Oxyfluoride Cathodes. Advanced Science, 2015, 2, 1500128.	5.6	56
110	Pd hydride and carbide studied by means of Pd K-edge X-ray absorption near-edge structure analysis. Bulletin of the Russian Academy of Sciences: Physics, 2015, 79, 1180-1185.	0.1	9
111	X-ray spectral diagnostics of synthetic lanthanide silicates. Optics and Spectroscopy (English) Tj ETQq1 1 0.7843	14 rgBT /0 0.2	Dverlock 10
112	X-ray absorption spectroscopy determination of the products of manganese borohydride decomposition upon heating. Bulletin of the Russian Academy of Sciences: Physics, 2015, 79, 139-143.	0.1	5
113	Optimized Finite Difference Method for the Full-Potential XANES Simulations: Application to Molecular Adsorption Geometries in MOFs and Metal–Ligand Intersystem Crossing Transients. Journal of Chemical Theory and Computation, 2015, 11, 4512-4521.	2.3	179
114	X-ray absorption spectroscopy with time-tagged photon counting: application to study the structure of a Co(i) intermediate of H2 evolving photo-catalyst. Faraday Discussions, 2014, 171, 259-273.	1.6	37
115	Oxidation state and local structure of a high-capacity LiF/Fe(V2O5) conversion cathode for Li-ion batteries. Acta Materialia, 2014, 68, 179-188.	3.8	9
116	Temperature- and Pressure-Dependent Hydrogen Concentration in Supported PdH _{<i>x</i>} Nanoparticles by Pd K-Edge X-ray Absorption Spectroscopy. Journal of Physical Chemistry C, 2014, 118, 10416-10423.	1.5	83
117	Electronic and Geometric Structure of Ce ³⁺ Forming Under Reducing Conditions in Shaped Ceria Nanoparticles Promoted by Platinum. Journal of Physical Chemistry C, 2014, 118, 1974-1982.	1.5	34
118	Pump-Flow-Probe X-ray Absorption Spectroscopy as a Tool for Studying Intermediate States of Photocatalytic Systems. Journal of Physical Chemistry C, 2013, 117, 17367-17375.	1.5	31
119	Spin-polarized electronic structure of the core–shell ZnO/ZnO:Mn nanowires probed by X-ray absorption and emission spectroscopy. Journal of Analytical Atomic Spectrometry, 2013, 28, 1629.	1.6	11
120	Synthesis and Characterization of MnCrO4, a New Mixed-Valence Antiferromagnet. Inorganic Chemistry, 2013, 52, 11850-11858.	1.9	8
121	Incorporation of nitrogen in Co:ZnO studied by x-ray absorption spectroscopy and x-ray linear dichroism. Physical Review B, 2013, 87, .	1.1	9
122	Local surrounding of vanadium atoms in CuCr1 â^' x V x S2: X-ray absorption spectroscopy analysis. Optics and Spectroscopy (English Translation of Optika I Spektroskopiya), 2013, 114, 397-400.	0.2	2
123	Local Atomic and Electronic Structure of the Fe dopants in AlN:Fe Nanorods. Journal of Physics: Conference Series, 2013, 430, 012112.	0.3	0
124	Application Ce L ₁ HERFD XAS to determine the atomic structure of CeO ₂ based nano-catalysts under working conditions. Journal of Physics: Conference Series, 2013, 430, 012062.	0.3	4
125	X-ray and electron spectroscopy investigation of the core–shell nanowires of ZnO:Mn. Solid State Communications, 2011, 151, 1314-1317.	0.9	13
126	Copper defects inside AlN:Cu nanorods – XANES and LAPW study. Journal of Physics: Conference Series, 2009, 190, 012136.	0.3	5

#	Article	IF	CITATIONS
127	Analysis of the local atomic structure of aluminum nitride nanoparticles. Journal of Surface Investigation, 2009, 3, 460-463.	0.1	5
128	Local and electronic structure of tribological materials: XANES analysis. Journal of Physics: Conference Series, 2009, 190, 012072.	0.3	0
129	Nitrogen defect levels in InN: XANES study. Radiation Physics and Chemistry, 2006, 75, 1635-1637.	1.4	3